

# Time simulation of squeal phenomena in realistic brake models

**G. Vermot des Roches<sup>1,2</sup>, E. Balmes<sup>1,2</sup>, T. Pasquet<sup>3</sup>, R. Lemaire<sup>3</sup>**

<sup>1</sup> Ecole Centrale Paris, Laboratoire MSS-MAT, CNRS UMR 8579  
Grande Voie des Vignes, 92295, Chatenay-Malabry, France

<sup>2</sup> SDTools

44, Rue Vergniaud, 75013, Paris, France

**vermot@sdtools.com balmes@sdtools.com**

<sup>3</sup> Bosch (Chassis Systems Brakes),

126, Rue de Stalingrad, 93700, Drancy, France

**Thierry.Pasquet@fr.bosch.com Remi.Lemaire@fr.bosch.com**

## Abstract

This paper presents a modeling strategy employed to obtain converged results on long time simulation of complex finite element brake models. First a novel reduction method, adapted to models showing large interface DOF, is presented. The small finite element area in the vicinity of the contact is treated as fully non-linear and while the remaining of the structure is represented by a superelement. The method is thus suited for large finite element models. A time integration scheme, based on a non-linear Newmark, is then adapted to allow large models to be computed over long time periods. This is achieved mainly by the use of a fixed iteration operator throughout the simulation. This technique is applied first to a simplified brake model for validation purposes, then to a state-of-the-art brake model designed by Bosch Chassis Brake Systems. The simulation results are put in perspective with recent publications on the subject.

## Introduction

The work presented in this paper seeks to introduce time simulation of brake instabilities on industrial brake models. Brake squeal corresponds to instabilities that generate high frequency vibrations (from 1 to 16 kHz) leading to unpleasant noises up to 120 dB in the brake vicinity, at low speed, low pressure braking cases which mostly happen in urban areas. Although the brake efficiency is not challenged, brake squeal is an important source of negative customer feedback and therefore needs to be avoided. In addition, new constraints on brake design involve strong weight restrictions and efficiency improvement so that squeal occurrences are even more difficult to handle.

The current industrial practice in numerical simulation for brake squeal is the study of complex mode stability [1, 2, 3]. This considers a linearization of the system equations around a stationary static state and evaluates stability in the sense of Lyapunov.

One of the drawbacks of these methods is that unstable complex modes only provide potential unstable modes. In the best case, only some of these modes are actually found to generate squeal instabilities. Time simulations have the potential to really describe the non-linear oscillations found after the instability induces a divergence from the stationary static state. They can thus be expected to allow an effective discrimination between the modes that are effectively leading to instabilities and those that are not destabilized in practice. Such method was successfully applied to train brake models in [2] by tracking unstable complex modes contribution to the time response.

Previous work on the time simulation of squeal (see [4, 2] for example) has been focused on somewhat simplified models, which do not account for the full geometrical complexity of actual brakes. Experiments on real brakes do however show a strong sensitivity on the actual brake configuration: details of the pad geometry, spring connectors, ... The first objective of this work is thus to introduce a practical methodology to allow time simulations for brake models that have high levels of details. The associated model reduction methodology is introduced in section 1.

The second issue is linked to the time integration over long intervals of problems with contact and friction. Treating non-linear systems usually challenges the convergence results obtained with linear systems, as shown in [5]. The use of a modified non-linear Newmark scheme adapted to contact formulations presented in section 2 has two main advantages. It allows larger than usual models (50,000 DOF) to be treated over 200,000 time steps. It also solves some of the convergence issues encountered with more classical schemes. In particular, the 'bouncing behavior' of the basic Newmark scheme is addressed. These results are illustrated using a simplified brake model as a demonstrator. Eventually, section 3 presents numerical results of squeal simulation on the industrial brake model provided by Bosch Chassis Brake Systems.

The proposed methodology is validated on both simplified and realistic brake models shown in figure 1. The simplified model consists of a cylindrical disc, with two cylindrical section shaped pads. The pads are guided in vertical translation at both edges, the disc is linked to the ground by springs fixed at the central inner nodes. A uniform pressure is applied to the pad backplates. The model shown is meshed using 8 node hexahedrons but other shapes and incompatible meshes have also been considered.

The realistic brake model conforms to a design from Bosch. It is composed of 8 components, the disc, outer and inner pads, anchor, caliper, piston, hub and knuckle modeled using the finite element method. Since brake squeal can reach high frequencies, the mesh is rather fine, which leads to approximately 600,000 DOF. The different components are in contact with each other and an exponential contact force is assumed. The parts too small to model such as the hub bearing, the pad springs, piston seal and boots are replaced by equivalent stiffness.

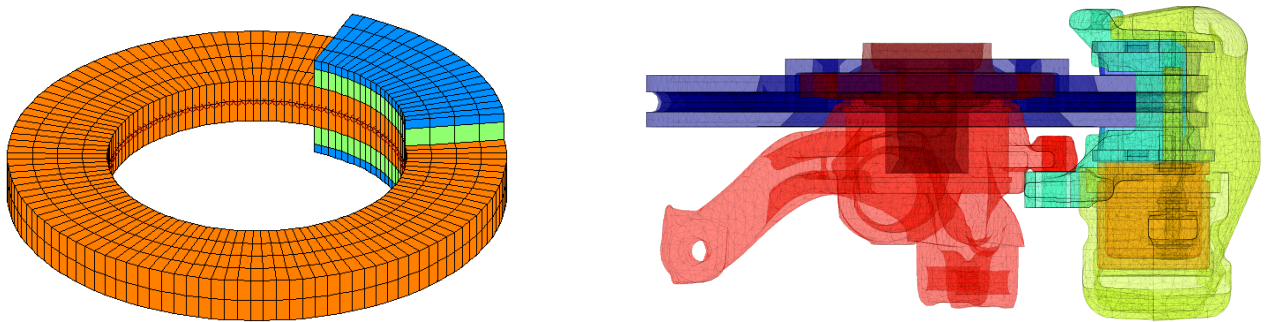


Figure 1: Finite element models of a simplified and a realistic brake

## 1 Reduction method for a system with local non-linearities

This section presents a novel reduction method adapted for finite elements models showing large interfaces. Indeed, classical reduction methods usually keep the interface DOF explicitly, thus generating potentially large full blocks in the resulting system matrices. This proves to be computationally inefficient and motivates the introduction of a method implicitly eliminating interface DOFs.

Component Mode Synthesis methods have traditionally been based on the assumptions [6] of component independence (reduction of a component is performed without knowing the others), static solution capability (static responses to applicable loads, in particular interface loads, are included explicitly), explicit boundary coordinates (in order to ease direct stiffness assembly).

When these methods were developed in the 70's, the objectives were linked to numerical performance and the ability to couple test and analysis models. The context of the proposed application is quite different. The objective is to reproduce the dynamics and steady state static response of the full brake model as closely as possible, while retaining the ability to account for the local non-linearities in the model. In application to brake squeal the disc/pad contact area is of great importance since it is the location where the instability originates. One thus chooses to keep all DOFs  $q_c$  of elements connected to the contact area explicitly, as shown in figure 2.

To achieve the first objective, one proposes to use a Rayleigh-Ritz method that use full system modes  $\phi_{1:NM}$  and the steady state response  $q_0$  as assumed shapes. To be compatible with the retention of all contact area DOFs, the modes are only assumed on DOFs  $q_b$  of the reduced part. In other words one considers the reduced basis

$$\begin{Bmatrix} q_b \\ q_c \end{Bmatrix} = \begin{bmatrix} [[\phi_{1:NM}]_b & q_{0b}] & 0 \\ 0 & [I]_c \end{bmatrix} \begin{Bmatrix} q_r \\ q_c \end{Bmatrix} \quad (1)$$

A Craig-Bampton reduction would proceed very differently. The DOFs to be retained explicitly would be divided in two sets:  $c_i$  for those part of elements connected to the reduced area and  $c_c$  for those purely internal to the unreduced part of the model. The reduction would then consider

$$\begin{Bmatrix} q_b \\ q_{c_i} \\ q_{c_c} \end{Bmatrix} = \begin{bmatrix} [\phi_{Fixed}] & -K_{cc}^{-1}K_{cc_i} & 0 \\ 0 & I & 0 \\ 0 & 0 & I \end{bmatrix} \begin{Bmatrix} q_r \\ q_{c_i} \\ q_{c_c} \end{Bmatrix} \quad (2)$$

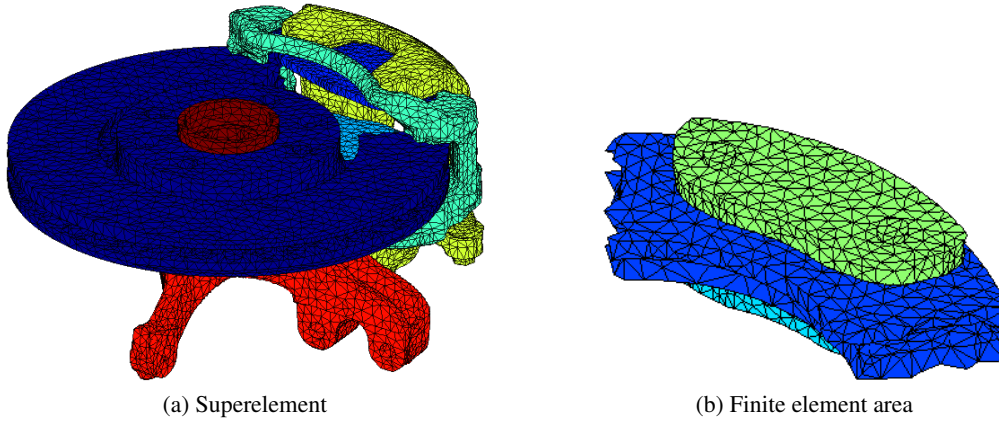


Figure 2: Brake model split in SE and kept area

In the present case, 250 modes, corresponding to a 20 kHz cutoff, are kept for the superelement reduction. In figure 3 one clearly distinguishes DOFs associated to the unreduced part of the disk, the two pads and the reduced component. The contact stiffness terms clearly couple the disk and the pads. With reduction basis (1), the reduced component is coupled with the unreduced part on the  $b, c$  block, which is small (251 : the number of considered modes + one static shape). In the Craig-Bampton approach, figure 3b, the coupling occurs for the  $c_i, c_c$  block which for linear tetra4 elements already represents 1765 elements (11,200 for tetra10). A clear advantage is obtained in terms of memory. The number of non null terms increases from 1 million with the new method to 8 millions with the classical Craig Bampton.

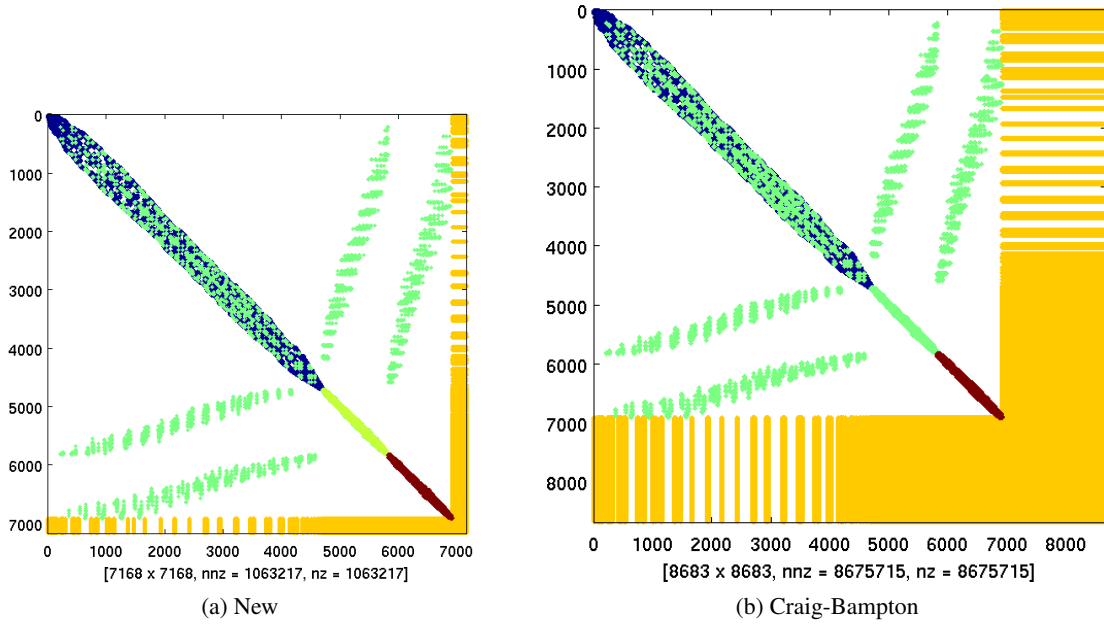


Figure 3: Reduced matrix topologies for the tetra4 model. Left proposed reduction. Right : Craig-Bampton reduction

Another advantage of the proposed reduction is that the real modes of the full model and the ones of the reduced model are theoretically identical. Here, a slight error is introduced in the realistic brake model due to differences in the contact handling between the Abaqus static step and the SDT time integration.

## 2 Time integration of the non-linear contact/friction model

Many numerical applications of contact resolution methods are targeting relatively small models. The optimization needed to handle large models has specificities which need to be addressed. This section presents the models, the contact and friction laws, a non-linear modified Newmark scheme based on [7] put in the contact perspective and eventually the damping strategy.

### 2.1 Contact laws

In a mechanical assembly, the components are in physical contact with each other. Penetration is defined as the relative displacement along the normal  $N$  of master and slave surfaces with a possible offset  $g_0$

$$\{g\} = N \cdot (u_{slave} - u_{master}) - \{g_0\} \quad (3)$$

The Signorini contact law represents the normal contact behavior between two solids and is plotted in figure 4a. The ideal Signorini contact shows no penetration and repulsive contact forces, written as a pressure  $p\{N\}$ , which are null when no contact occurs

$$\begin{cases} g \leq 0 \\ p \leq 0 \\ (g) \cdot (p) = 0 \end{cases} \quad (4)$$

An exact implementation of the Signorini equations can be obtained with a Lagrange formulation that keeps the contact forces as unknowns and solves a coupled displacement/force problem. This method is not chosen

here due to the increased DOF number for a large contact area and the difficulty to implement it properly in dynamics. An solution would however be the non-smooth contact dynamics method suggested in [8] and applied successfully for brake squeal simulation in [2].

Penalization methods introduce a relationship between the gap and the contact pressures. An exponential law is considered here,

$$p(g) = p_0 e^{-\lambda g} \quad (5)$$

In brakes, rough surfaces are contacting. A Signorini contact would thus be an idealization valid for very stiff contact stiffness between the asperities. The exponential contact law is another idealization and it is quite difficult to rank their relative validity. Experiments have however led Bosch to consider that  $p_0 = 10^{-2} MPa$  and  $\lambda = 750 mm^{-1}$  are realistic values for disk/pad contact. The perspective that this exponential law is a regularization of the Signorini contact law is classical, but not necessarily valid here.

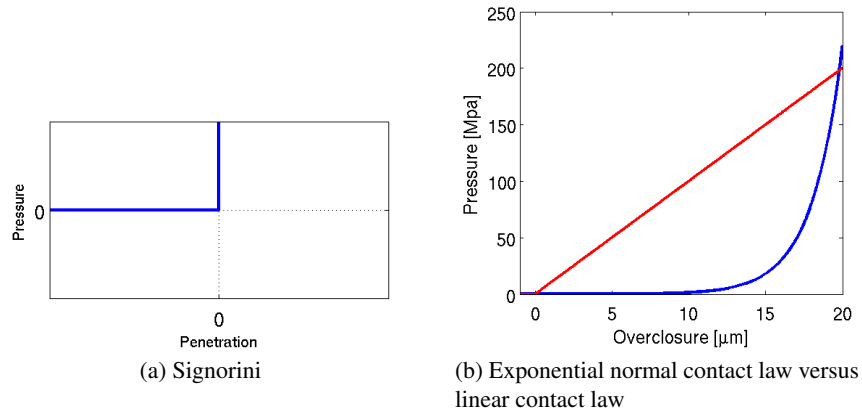


Figure 4: Contact laws, Signorini and regularizations

This contact formulation is applied to a finite element model by pairing a master surface which contains contact integration points and a slave surface. The contact points of the master surface are paired with the nodes of the slave surface to define the model displacement formulation. The contact forces are used directly in the formulation (section 2.3). They are computed at the integration points using Gauss weighting coefficient and the element contact force density.

$$\{\hat{q}\}^T \{f_N\} = \int \{\hat{u}\}^T N p dS \simeq \sum_j \{\hat{u}\}^T \{N\} p(x_j, q) \omega_j J(x_j) \quad (6)$$

where  $f_N$  is the global contact force,  $p$  the contact pressure,  $x_j$  are the integration points,  $\hat{q}$  a virtual displacement,  $q$  the displacement and  $J(x_j)$  the jacobian of the shape transformation (surface associated with integration point).

At a contact integration point, a contact stiffness can be defined as the derivative of the contact pressure

$$k_c(g) = \frac{\partial p}{\partial g} = \lambda p_0 e^{-\lambda g} \quad (7)$$

This leads to a contact stiffness matrix given by

$$\begin{aligned} \{\hat{q}\} [K_c] \{q\} &= \int \{\hat{u}(\hat{q})\}^T \{N\} \lambda p_0 e^{-\lambda g} \{u(q)\}^T \{N\} dS \\ &\simeq \sum_j \{\hat{u}\}^T \{\hat{u}(\hat{q})\}^T \{N\} \lambda p_0 e^{-\lambda g} \{u(q)\}^T \{N\} \omega_j J(x_j) \end{aligned} \quad (8)$$

## 2.2 Friction laws

The Coulomb law describes the tangential contact behavior in the presence of friction. The sliding velocity  $w_s$  is defined as the relative speed between the two bodies in contact. the contact force is split into a normal contact force  $F_N$  and a tangential contact force  $F_T$  that one links using the friction coefficient  $\mu$ .

$$\begin{cases} \|F_T\| \leq \mu \|F_N\| & w_s = 0 \\ \|F_T\| = \mu \|F_N\| & \exists A \geq 0, w_s = -AF_T \end{cases} \quad (9)$$

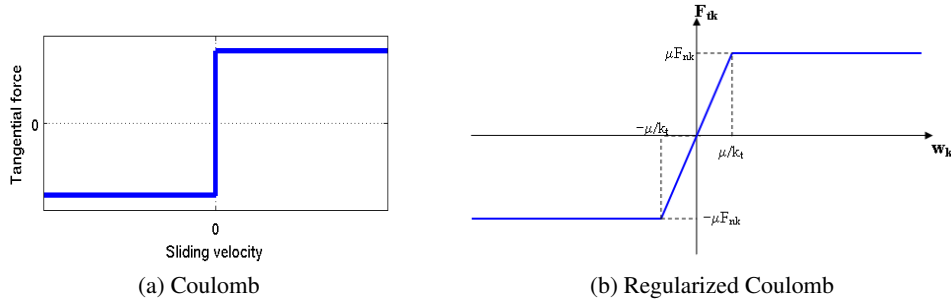


Figure 5: The Coulomb contact laws

In application to brake squeal, a monodirectional contact force, along  $\theta$  in cylindrical coordinates, is computed. The Coulomb law is regularized by assuming a permanent sliding state, and penalizing small sliding velocities as shown in figure 5b and written as

$$\begin{cases} \|F_T\| = k_t \|w_s\| & \text{if } \|w_s\| < \frac{\mu}{k_t} \\ \|F_T\| = \mu \|F_N\| & \text{else} \end{cases} \quad (10)$$

Actual materials used in the car industry show a friction coefficient of  $\mu = 0.6$  which was used for this study. The choice of  $k_t$  is still opened, it was taken as  $k_t = 50s^{-1}$ .

## 2.3 Time integration scheme

A modification of the non linear, displacement based, Newmark scheme presented in Ref. [7] is considered here. The scheme, shown in figure 6, is classically divided in an external time incrementation loop with a prediction phase and an internal non linear correction phase. The Newmark coefficients noted  $\beta = \frac{1}{4}$  and  $\gamma = \frac{1}{2}$  are kept as usual.

The correction phase is performed with a Newton scheme where the residual (14) is computed with the contact forces  $F_N$  and  $F_T$  and the correction is given by (15). In a standard Newton scheme, the Jacobian corresponds to sensitivity of the residual with respect to a change in the unknown, taken here to be the position,

$$[J(q)] = \frac{\partial r}{\partial \delta q} = [K_{el}] + [K_c(q)] + \frac{\gamma}{\beta h} [C] + \frac{1}{\beta h^2} [M] \quad (11)$$

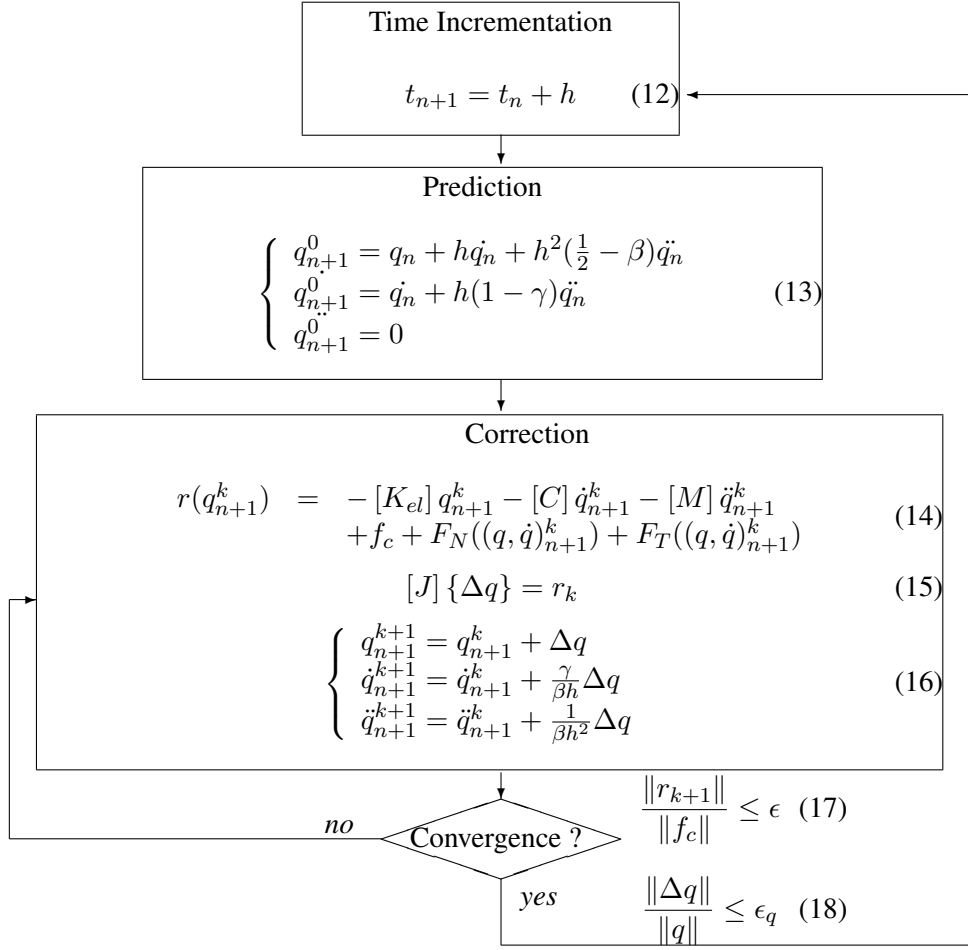


Figure 6: Non-linear Newmark scheme

Considering a variable jacobian  $[J]$  is impractical. The reduced brake model presented in section 1 has around 50,000 DOF, and 200,000 time steps are needed. Since the best jacobian factorization time for such matrix is of the order of 10 seconds, even a single factorization by time step would require over a thousand hours of computation. Besides, the very soft behavior of the exponential contact law shown in figure 4b may cause divergence for low overclosures.

The Newton scheme is thus modified to use a constant jacobian. In (11), one introduces a constant reference contact stiffness by replacing  $[K_c(q)]$  by  $k_c [K_c]$ , where  $[K_c]$  is the contact coupling matrix for a unity contact stiffness. The scalar value of the contact stiffness  $k_c$  is then optimized to ensure convergence speed.

The adjustment of  $k_c$  is illustrated, in figure 7, for the simplified brake model and an exponential law (presented in section 2.1). For a small  $k_c$ , divergence (set at 200 iterations) occurs. As  $k_c$  is increased oscillations are found. This can be linked to examples given in the litterature (e.g. in [5]) of bouncing effects when the integration scheme fails to converge without explicitly diverging. An optimum  $k_c$  value clearly appears in the second graph of figure 7, just after convergence is met.

Although the jacobian has to be optimized, its effect is mostly observed during the static computation. Indeed, the time steps used for a squeal simulation are very low, which combined to the displacement increment convergence criterium, yields a limited number of Newton iterations. Getting the right order for  $k_c$  is usually enough. The value used for the realistic brake model is 185 MPa.

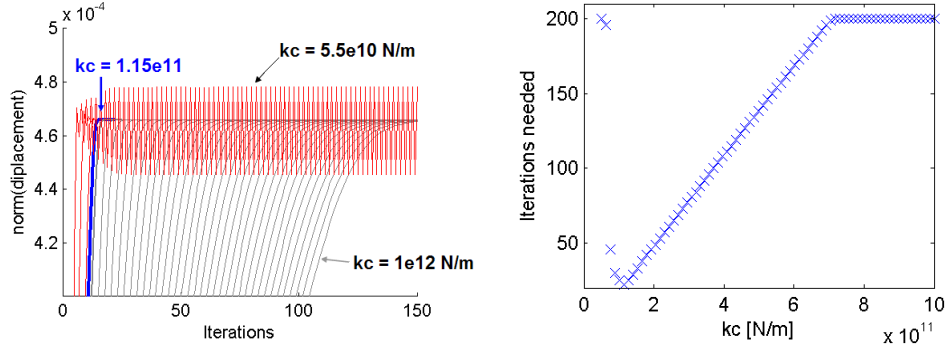


Figure 7: Static state convergence as function of  $k_c$  on a simplified brake model

*A posteriori*, it was found that the optimum value is close to the average tangent stiffness value at the equilibrium. Since the jacobian is constant, it corresponds to the direct path to the solution. The contact distribution is not evenly distributed so a few iterations are still needed to find the real contact distribution from an averaged state.

The convergence criterion (17) is another key point since a poor choice may lead to numerous costly Newton iteration when the displacement is close to the solution. An alternative is to combine it with a displacement convergence test in equation (18), which considers that convergence is achieved if a negligible Newton displacement increment happens. In most cases, it decreases the number of Newton iteration needed by time step, but it must be used carefully since it overrides the verification of the mechanical equilibrium (equation (14)). In practice, a convergence criterion on the displacement increment was chosen with a tolerance of  $\epsilon_q = 10^{-6}$ .

## 2.4 Damping

Using a Rayleigh damping formulation, the notion of contact damping can be introduced. The contact stiffness can be segregated from the stiffness matrix and therefore be applied a specific coefficient.

$$[C] = a [M] + b [K_{el}] + \tilde{b} [K_c] \quad (19)$$

where  $[M]$ ,  $[C]$ ,  $[K_{el}]$ ,  $[K_c]$  are respectively the mass, damping, elastic stiffness and contact stiffness matrices,  $a = 0$ ,  $b = 2.12 \cdot 10^{-7}$  and  $\tilde{b} = 0$  are parameters set here for only high frequency damping.

The use of (19) yields the jacobian formulation used in this paper, written in equation (20). No numerical damping is used.

$$[J] = \left(1 + \frac{\gamma b}{\beta h}\right) [K_{el}] + k_c \left(1 + \frac{\gamma \tilde{b}}{\beta h}\right) [K_c] + \left(\frac{1}{\beta h^2} + \frac{\gamma a}{\beta h}\right) [M] \quad (20)$$

Contact damping is stated to be of importance in [2], none was used in the presented study since it did not correlate to any obvious physical meaning.

### 3 Time simulation results

This section presents squeal simulations obtained with a simplified brake for convergence validations and a realistic brake. The results are related to common phenomena observed in other works.

#### 3.1 Validations on a simplified brake model

The simplified brake model illustrated in the introduction is meshed in 8 nodes hexahedrons elements. The disc and backplate are elastic isotropic, the lining is transverse anisotropic, using the materials of the realistic brake. To trigger the instability, a pressure shock is applied at the beginning of the simulation (a 10% overpressure during the first  $10^{-5}s$ ). A friction coefficient of 0.25 is applied.

The time scheme convergence is assumed when reducing the time step does not change the solution. Figure 8 and 9a shows that for  $dt \leq 10^{-7}s$ , the time responses are perfectly overlaying. This time step will be kept for the next simulations.

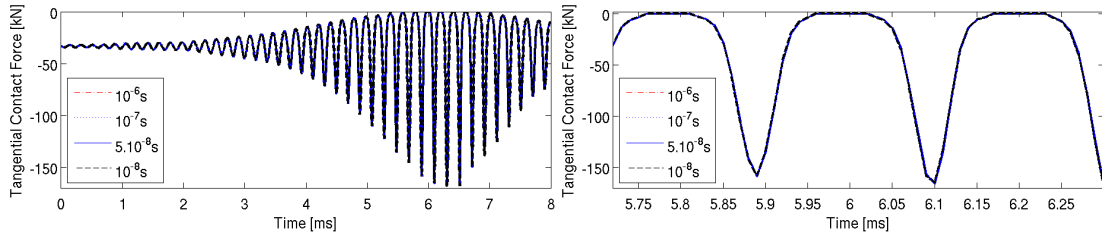


Figure 8: Time simulation on the simple model, as function of the time step

The Fast Fourier Transform (FFT) of the time response shows the instability frequencies. Figure 9a shows the FFT computed for the time simulation between 1 ms and 6 ms, which corresponds to the instability settling. A main instability frequency can be seen at 5.1 kHz with 3 harmonics.

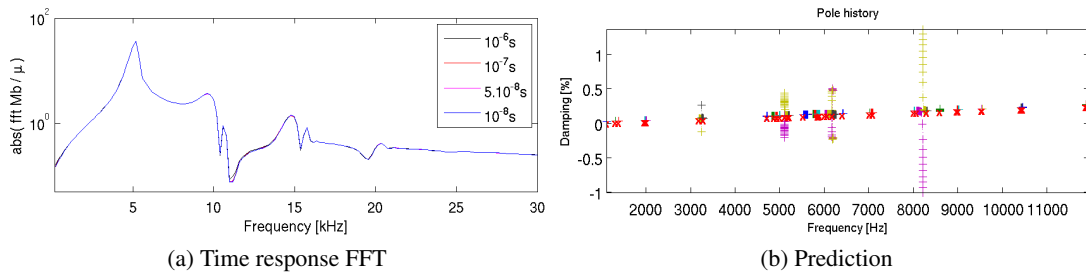


Figure 9: FFT of the time response between 1 and 6 ms, for various time steps, compared to the *a priori* stability diagram

In parallel, a stability diagram shown in 9b can be computed using the complex modes of the system linearized in the neighborhood of the periodic solution (which is also the initial condition for the time integration). The unstable modes are highlighted by plotting the complex poles for a friction coefficient varying from 0.01 to 0.5. 4 modes are found potentially unstable at 3.2, 5.1, 6.2 and 8.2 kHz.

The comparison of the two graphs of figure 9 first validates the time simulation by showing an instability happening at 5.1kHz corresponding to one of the modes predicted in the frequency domain. It also proves the interest of the time simulation since only one of the frequency domain unstable modes actually diverges.

The movement of the instability can be visualized using a waterfall plot as presented in figure 10a. The movement features a pumping pattern with a slight dephasing between the entry ( $+0.5 rad$ ) and the exit ( $-0.5 rad$ ) of the pad. Contact losses only happen at the exit of the pad; this is linked to an arching

phenomenon due to the disc rotation. Indeed the contact pressure is higher at the disc entry than at the exit, which

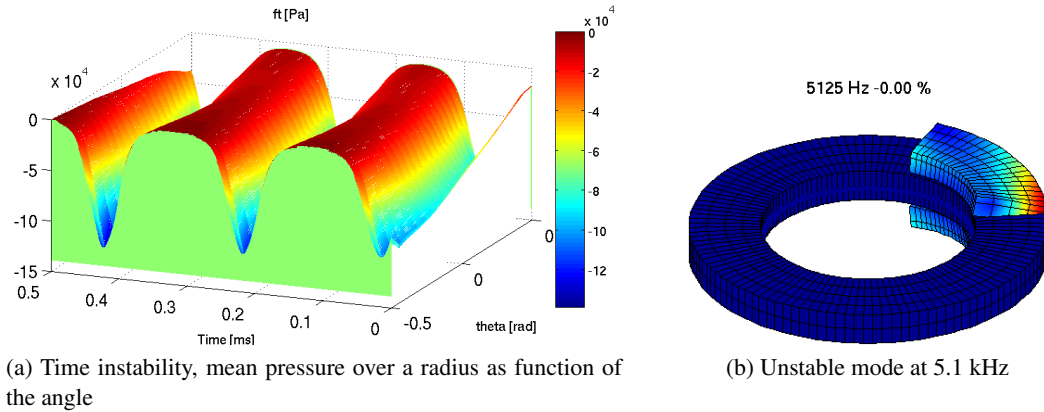


Figure 10: Pattern of the unstable mode found in the time simulation

### 3.2 Realistic brake simulation results

The real brake presented in 1 is meshed using 10 nodes tetrahedron elements. The friction braking pressure is set at 5 bar, and the disc angular velocity at  $5 \text{ rad s}^{-1}$  the friction coefficient is set at 0.6. The results presented in this section took 12 hours of computation (equally divided between displacement incrementation and residue computation). The use of the mkl library from intel has already cut the computation time by 30 %. The braking torque was taken as a reference signal to detect instability. Figure 11 shows the braking torque and the global friction coefficient.

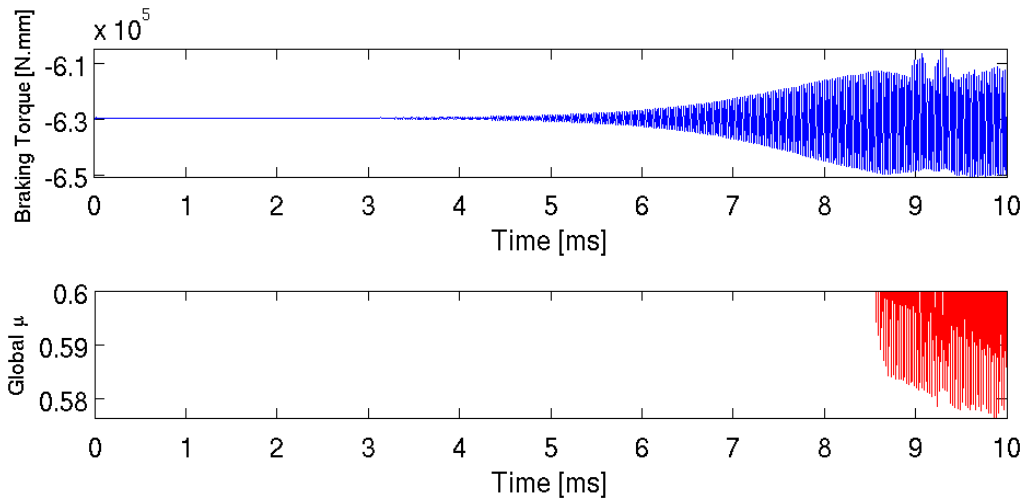


Figure 11: Result of the squeal simulation: braking torque and global friction coefficient

The braking torque shows the common limit cycle instability type. The stable periodic solution transits through an exponential divergence phase before the amplitude range settles to a bounded value. The global friction coefficient was computed; it is not constant. It is the ratio of the normal contact force resultant and the tangential force resultant over time. Although the local coefficient is set constant at 0.6, the measured  $\mu$  can decrease due to the loss of contact caused by the vibrations. This was also observed in [4]. Another illustration is given in figure 12 where the tangential contact force at an integration contact point is plotted.

Figure 12 highlights stick/slip transition by showing the sign switching of the contact force at a contact integration point. The stick property is not really implemented in the system although low sliding velocities

are penalized, it does not account properly for the phenomenon and yields very quick slip velocity direction switching.

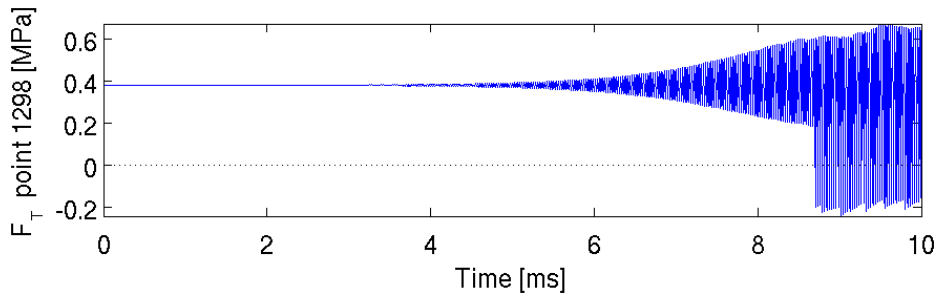


Figure 12: Tangential contact force at an intergration contact point

The frequency of instability is happening at 30 KHz, which is higher than the cutoff frequency retained for the superelement. Besides, there is very low damping in the system, it comes only from the Rayleigh damping, set a 1% at 15kHz. More damping must in fact be taken into account regarding the viscoelasticity of the lining material, the contact damping, the stick states, or the numerical high frequency damping. Their effect needs to be studied to obtain a better insight of the squeal instability.

Eventually, the precision of the static state input needs to be very accurate due to the use of an exponential contact law. At high contact pressures, coarse round-off errors should be avoided however, such accuracy was not achieved due to handling difficulties using Abaqus 6.6-1. Figure 13 shows the difference between the contact distribution proposed by Abaqus and SDT. Both solutions are computed from the static displacement output by Abaqus. The Abaqus solution corresponds to the contact forces recovered using the elastic stiffness matrix (without interaction) also output by Abaqus. The SDT solution corresponds to the contact forces computed from the Abaqus static displacement by using the analytical exponential contact law proposed in section 2.1 and the usual finite element shape function for 6 points triangles, using three contact integration points placed at the Gauss points.

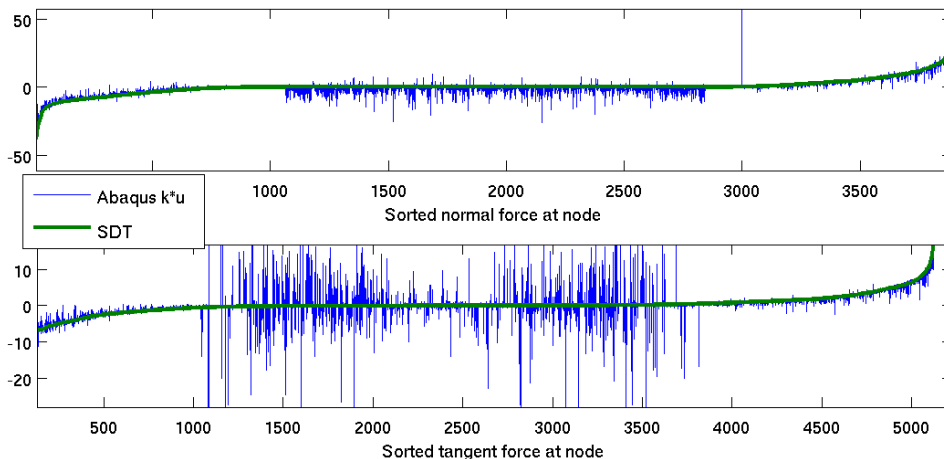


Figure 13: Differences between SDT and Abaqus. Contact points sorted by increasing value of the SDT solution, contact forces in N

None of the solutions shown are regular but great differences exists. In particular an outlier is detected in the Abaqus normal contact force solution. A lot of noise is seen on the tangential force with oscillations at the low contact area higher than the maximum contact force. This low level of accuracy obtained for the initial condition is also believed to play a role in the convergence difficulties experimented with the realistic brake model.

## Conclusion

This paper has proposed a time simulation of brake squeal applied to industrial brake models. First a novel reduction strategy was proposed to combine a non reduced finite element part around the pad/disc contact area and the superelement containing the system's remains. This method allows the interface DOF to be implicitly eliminated, thus avoiding large full blocks patterns obtained with a classical Craig-Bampton approach. Besides, the full and reduced real modes are identical. An improvement which may prove to be necessary is the implementation of a residual mode for precision; an automatic method is being developed to deal with some Abaqus implementation issues.

The time integration scheme proposed solves some common convergence issues acknowledged for the non-linear Newmark scheme. However, the brake instability caught in the time simulation is much higher than expected, and it has been found that the combination of a basic regularization of the Coulomb law (permanent sliding state, quick transitions) and the modified Newmark could yield numerical instabilities. The development of a Lagrangian tangential contact formulation is under development to improve the stick model. This would generate a hybrid contact law, using an exponential penalization formulation for the normal contact law, and a Lagrangian formulation for the tangential one. From the time integration point of view, alternative schemes will be tested in particular the modified  $\theta$ -method originally proposed in [8] and adapted in [2].

Further development will imply the implementation of richer damping models. Although literature concerning damping in time simulation is usually limited to numerical damping and Rayleigh damping, models from the frequency domain will be studied. First, time domain modal damping will be treated allowing to spread the damping to other interfaces in the superelement. It is based on the mass normalization of the modes constituting the reduction basis to recover the full damping matrix.

Viscoelastic damping will also be addressed to enrich mode pad lining material model. Such behavior has been acknowledged for this material only taken as elastic transverse anisotropic in this study. The formulation will be different from the one used in the frequency domain since the use of an imaginary matrix is impossible; a formulation featuring relaxation times would be preferred. Eventually, friction damping will be studied; its importance is highlighted in [2] for example, and a basic realization is suggested in this paper. Again, such damping will be prone to stabilize the stick/slip transitions by penalizing the sliding velocity.

## References

- [1] F. Moirot *Study of stability of an equilibrium in presence of Coulomb's friction. Application to disc brake squeal* ph.D Thesis (1998).
- [2] X. Lorang, *Instabilité vibratoire des structures en contact frottant: Application au crissement des freins de TGV*, ph.D Thesis (2007).
- [3] G. Fritz, J-J. Sinou, J-M. Duffal, L. Jézéquel, *Investigation of the relationship between damping and mode-coupling patterns in case of brake squeal*, Journal of Sound and Vibration, 6 November 2007, voluem 307, Issues 3-5, Pages 591-609.
- [4] V. Linck, *Modélisation numérique temporelle d'un contact frottant. Mise en évidence d'instabilités locales de contact - Conséquences tribologiques*, ph.D Thesis (2005).
- [5] B. Magnain, Z-Q. Feng, J-M. Cros, *Schéma d'intégration adapté aux problèmes d'impact*, Comptes Rendus Mécanique, Volume 333, Issue 5, May 2005, Pages 419-424.
- [6] R. Jr. Craig *A review of time-domain and frequency domain component mode synthesis methods* Int. J. Anal. and Exp. Modal Analysis, 1987, Volume 1, Pages 59-72.

- [7] M. Géradin, D. Rixen, *Mechanical Vibrations : Theory and Applications to Structural Dynamics*, Wiley Interscience, Second edition, 1996.
- [8] M. Jean, *The non-smooth contact dynamics method*, Computer Methods in Applied Mechanics and Engineering, 20 July 1999, Volume 177, Issues 3-4, Pages 235-357.